Applied Catalysis B: Environmental 150–151 (2014) 647–655

Contents lists available at ScienceDirect

Applied Catalysis B: Environmental

journal homepage: www.elsevier.com/locate/apcatb

Dispersion effects of Ni_2P catalysts on hydrotreating of light cycle oil

Gwang-Nam Yun, Yong-Kul Lee*

Laboratory of Advanced Catalysis for Energy and Environment, Department of Chemical Engineering, Dankook University, 126 Jukjeondong, Yongin 448-701, Republic of Korea

ARTICLE INFO

Article history:
Received 27 July 2013
Received in revised form 6 January 2014
Accepted 7 January 2014
Available online 17 January 2014

Keywords:
Light cycle oil
Ni_2P catalyst
Hydrotreating
HDS
HDN

ABSTRACT

A series of Ni_2P/SBA-15 catalysts with different Ni_2P loadings were prepared and applied for the hydrotreating of light cycle oil. The loading level of Ni_2P was varied from 0.5 to 3.0 mmol Ni_2P per 1.0 g of SBA-15 support, resulting in the optimum catalyst loading of 2.0 mmol Ni_2P. The physical properties of the catalyst samples were characterized by N_2-adsorption–desorption isotherms, CO uptake chemisorption, TPR, and TEM. X-ray diffraction (XRD) and extended X-ray absorption fine structure (XAFS) spectroscopy were used to obtain structural properties for the supported Ni_2P catalysts. Hydrotreating tests were performed in a continuous flow fixed-bed reactor at 623 K, 3.0 MPa, and LHSV's of 0.5–1.0 h^{-1}. The 2.0 mmol Ni_2P/SBA-15 gave an HDS conversion of 99.0% and an HDN conversion of 92.5%, which were much higher than those of a Ni–Mo–S/Al_2O_3 catalyst which gave an HDS conversion of 91.9% and an HDN conversion of 65.8% based on the same LHSV of 0.5 h^{-1}. Substantial changes in the composition of aromatic compounds were found for the Ni_2P/SBA-15 catalysts from 14.3 wt.% 1-Ar (mono-aromatics), 40.6 wt.% 2-Ar (di-aromatics) and 19.4 wt.% 3^+-Ar (tri$^+$-aromatics) in the LCO feed to 46.1 wt.% 1-Ar, 16.3 wt.% 2-Ar and 2.0 wt.% 3^+-Ar in the product.

1. Introduction

Light cycle oil (LCO) accounts for approximately 10–20 wt.% of the fluidized catalytic cracking (FCC) products and the stream has been used as low graded fuel additives due to its poor quality of low cetane number and high sulfur, nitrogen and aromatics contents [1]. In order to increase its use as a value-added diesel feedstock, a severe hydrotreatment is thus required [2–5]. Considering the high contents of heterocyclic compounds in LCO, the conventional hydrotreating catalysts may suffer from the competitive reactivity of hydrodesulfurization (HDS), hydrodenitrogenation (HDN), hydrodearomatization (HDA), and hydrocracking (HCK) [6–10]. The common hydrotreating catalysts are sulfided Co–Mo, Ni–Mo, and Ni–W. Co–Mo catalysts have higher HDS activity but with lower HDN and HDA activities than Ni–Mo and Ni–W catalysts [11]. One way to face these challenges is to develop alternative catalysts that can better withstand the severe operating conditions prevailed in the hydrotreatment process [12–15].

Recently, a new catalyst group of transition metal phosphides was introduced as a hydrotreating catalyst, which showed a good and stable catalytic activity for HDS and resistance to aromatic hydrocarbons and N-compounds [16,17]. Previous works have shown that MoP, WP, and Ni_2P have good activity in hydrotreating [18–21]. Among the phosphides, nickel phosphide (Ni_2P) has been found to be the most active and stable in the HDS and HDN [16,22]. A study on the effect of the Ni_2P dispersion on the hydrotreating performance with a high surface area silica (350 m^2 g^{-1}) and a mesoporous siliceous material (790 m^2 g^{-1}) (MCM-41) as supports proved that Ni_2P catalysts supported on high surface area MCM-41 support exhibited better HDS activity for a refractory sulfur compound than a Ni_2P/SiO_2 catalyst at 613 K and 3.0 MPa based on equal sites (230 μmol) loaded in the reactor [23]. The use of high surface area supports provided an opportunity to investigate the effect of particle size or dispersion on the HDS and HDN activity, which demonstrated that the higher dispersion of Ni_2P catalyst gave the better catalytic activity for HDS and HDN[24].

Although much research has been made for the phosphide catalysts on the hydrotreating of diesel feedstocks, little work has been reported on the hydrotreating of LCO [17,25–29]. In the present study, we focused on preparing different loading levels of Ni_2P catalysts on high surface area SBA-15 support to examine the effect of Ni_2P dispersion on the hydrotreating of light cycle oil as a real feedstock.

2. Experimental

2.1. Synthesis of supported Ni_2P catalysts

Commercial SiO_2 supports (Cabot, Cab-O-Sil) was used as received. A mesoporous SBA-15 silica support was synthesized

* Corresponding author. Tel.: +823180053466.
E-mail address: yolee@dankook.ac.kr (Y.-K. Lee).

0926-3373/$ – see front matter © 2014 Elsevier B.V. All rights reserved.
http://dx.doi.org/10.1016/j.apcatb.2014.01.010

by following a procedure in literature [30,31]. Supported Ni_2P catalysts were prepared by incipient wetness impregnation of aqueous metal phosphate precursors, followed by temperature programmed reduction (TPR) in flowing hydrogen. The initial Ni/P ratio in the precursors was fixed at 1/2. The amount of Ni loading was varied: 0.5, 1.0, 1.5, 2.0, and 3.0 mmol/g of support. The supported nickel phosphate precursor was prepared by incipient wetness impregnation of a solution of nickel nitrate, $Ni(NO_3)_26H_2O$ (Alfa Aesar, 98%) and ammonium phosphate $(NH_4)_2HPO_4$ (Samchun, 99%), followed by drying at 393 K for 7 h and calcination at 673 K for 4 h. The resulting precursor phosphates were reduced to the corresponding phosphides by TPR from 298 to 873 K (at 1 K min^{-1}) in quartz U-tube reactors using hydrogen flow of 100 cm^3 min^{-1}. After reduction, the phosphides were cooled to room temperature under 100 cm^3 min^{-1} helium flow and typically were passivated under 0.2% O_2/He flow (100 cm^3 min^{-1}) for 4 h. For comparison, Co–Mo–S and Ni–Mo–S/Al_2O_3 catalysts were also prepared. The Ni–Mo/γ-Al_2O_3 and Co–Mo/γ-Al_2O_3 catalysts used in this work contained 10 wt.% Mo and 3 wt.% promoter (Ni or Co). They were prepared by incipient wetness impregnation of γ-Al_2O_3 (Alfa Aesar, 99.9%, metals basis) with an aqueous solution of $(NH_4)_6Mo_7O_{24}{\cdot}4H_2O$ (Samchun, 99%), followed by an aqueous solution of $Ni(NO_3)_2{\cdot}6H_2O$(Alfa Aesar, 98%) or $Co(NO_3)_2{\cdot}6H_2O$(Kanto, 99.9%). After each impregnation step the catalysts were dried overnight at 393 K and calcined at 773 K for 2 h.

2.2. Characterization of catalyst samples

The temperature programmed reduction (TPR) technique was used to identify the reduction characteristics of the material. 0.20 g of material was loaded in a quartz glass U-tube reactor and the effluent was monitored by a mass spectrometer (HP 5973 inert). CO chemisorption uptake was measured on passivated samples re-reduced in situ in a H_2 flow (100 cm^3 min^{-1}) at 723 K for 2 h before the measurements. Pulses (100 μmol) of CO at room temperature (300 K) were passed over the sample to measure the total dynamic gas uptake. A Micromeritics ASAP 2010 micropore size analyzer was used to measure the specific surface area of the sample from the linear portion of BET plots (P/Po = 0.01–0.10) at 77 K. TGA measurements were carried out on a SDT 2960 (TA instruments) and alumina pans. About 10 mg of each sample was equilibrated at 313 K for 5 min and then heated from 313 K to 1063 K with a heating rate of 10 K min^{-1} under nitrogen atmosphere and nitrogen gas flow of 50 cm^3 min^{-1}.

Table 1
Composition and properties of light cycle oil (LCO).

Physical properties		LCO
API		13.5
S/ppm		3930
N/ppm		550
Color (ASTM)		L2.5
Aromatics/wt.%	Total	74.3
	Mono	14.3
	Di	40.6
	Tri	19.4
Cetane index		24.9
Distillation/K	IBP/5/10	498/529/535
	30/40/50	557/565/581
	60/90/95	598/671/–
	EP	–

The chemical composition of the samples was determined by inductively coupled plasma–atomic emission spectroscopy (ICP–AES) (PerkinElmer, Model Optima-4300 DV). HR-TEM images were obtained using a JEM-2100F, 200 kV microscope. X-ray absorption spectra at the Ni K-edge (8.333 keV) of the reference and catalyst samples were recorded in the energy range 8.233–9.283 keV using synchrotron radiation at the beamlines 7D and 10 C of the Pohang Light Source (PLS). The X-ray ring at the PLS has a flux of 5×10^{12} photons s^{-1} at 100 mA and 3 GeV. The X-ray single crystal at the beamline 10 C is equipped with a Si (1 1 1) channel-cut monochromator and has an energy range capability of 4–22 keV. The samples were prepared in a kapton sealed glass cell to avoid air-exposure. The X-ray absorption spectra were recorded at ambient temperature in transmission mode using ionization chambers for the detection of primary (I_0, 100% N_2) and transmitted (I_T, 100% N_2) beam intensities. The obtained XAFS data were analyzed by Winxas 3.1.

2.3. Activity test for hydrotreating of light cycle oil

The catalytic tests of hydrotreating were carried out in a continuous-flow reactor (catalyst loaded with 1.0 cm^3) as displayed in Scheme 1 at 3.0 MPa and 623 K. Before injecting the reactant, the catalysts were activated in situ under H_2 flow of 100 cm^3 min^{-1} (99.999%) at 723 K for 2 h to remove the oxygen from the surface. The sulfide catalysts were pretreated at 573 K for 2 h with 100 cm^3 min^{-1} of 10% DMDS/H_2 at 1 atm. Light cycle oil was supplied from a refinery in Korea. The specifications of the light cycle oil used in this study are summarized in Table 1. The light

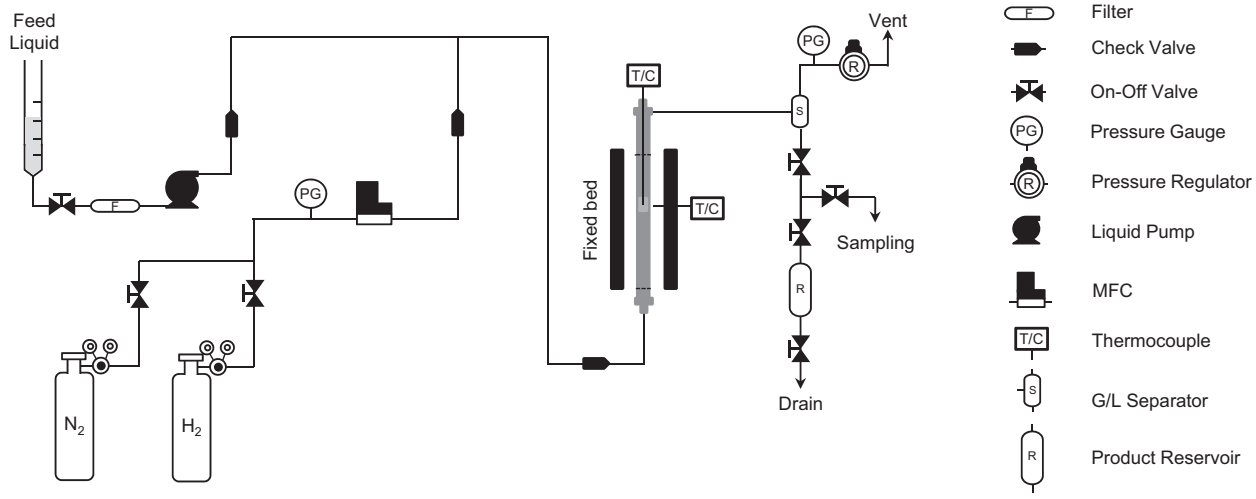

Scheme 1. Schematic of hydrotreating unit.

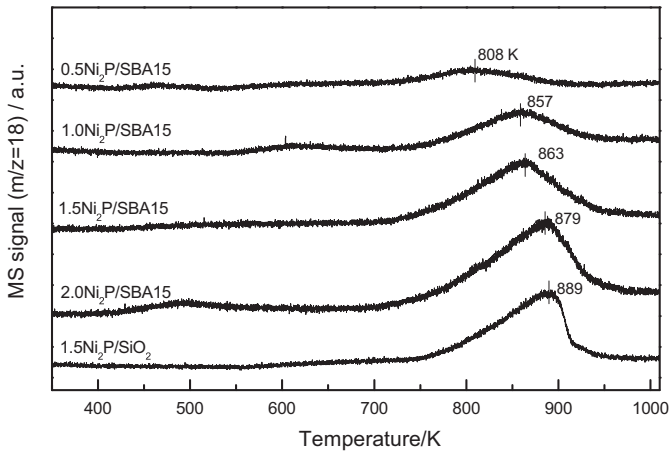

Fig. 1. TPR profiles of oxidic precursors of the supported Ni_2P catalyst samples.

cycle oil was fed to the reactor by means of a liquid pump at 0.5 $cm^3\ h^{-1}$ for 25 h and 1.0 $cm^3\ h^{-1}$ for 20 h in series to obtain LHSV of 0.5 and 1.0 h^{-1}, respectively, along with 500 $cm^3\ min^{-1}$ of hydrogen flow. Liquid product compositions were analyzed by a gas chromatograph equipped with a pulsed flame photometric detector (Agilent-6890-PFPD, HP-1, Cross linked methyl silicone gum, 25 m × 0.32 mm × 0.17 μm) to characterize the distribution of sulfur compounds between different classes, on samples collected at 4 h intervals. The total nitrogen content of the liquid product was measured by combustion/chemiluminescence technique following ASTM D4629 method, and the sulfur content was measured using combustion/fluorescence technique following ASTM 5463 procedure. Both sulfur and nitrogen were analyzed in an Antek 9000 NS analyzer. The HDS and HDN conversions were defined as percent of total S and N removed from the initial light cycle oil. Polycyclic aromatic hydrocarbons were monitored and quantified by high-pressure liquid chromatography with fluorescence detection (HPLC–FD).

3. Results and discussion

3.1. Effect of Ni_2P loading on catalyst dispersion and structure

The supported Ni_2P catalysts were prepared by the temperature-programmed reduction (TPR) of supported nickel phosphate precursors. Fig. 1 shows the TPR profiles of the calcined phosphate precursors of the Ni_2P catalyst samples. A distinct reduction feature at around 750–950 K with a peak close to 870 K is observed with the peak maximum shifting to slightly higher temperature and the peak being more broadened for the samples with higher loadings, indicating a longer diffusion path for the removal of oxygen in the larger particles.

Fig. 2 shows the powder XRD patterns of the fresh and spent Ni_2P catalyst samples and a bulk Ni_2P reference. The broad line centered at $2\theta = 22^\circ$ is typical for amorphous silica, which is observed in all case the patterns. The diffraction pattern for Ni_2P/SiO_2 shows three main peaks at 40.5°, 44.8° and 47.5°, corresponding to the characteristic XRD peaks of bulk Ni_2P reference. The characteristic XRD signals of Ni_2P on the SBA-15 supports are visible for the samples with higher loadings of 1.5, 2.0 and 3.0 Ni_2P. For the samples with lower loading levels of 0.5 and 1.0 Ni_2P/SBA-15 characteristic peaks for a Ni_2P phase were very weak, and became invisible after reaction, indicating that crystallite size is below 0.4 nm. In the case of the 1.5, 2.0, and 3.0 Ni_2P/SBA-15, the retention of the Ni_2P peaks even after reaction indicates that the Ni_2P phase does not deteriorate. For the samples with same loading levels of 1.5

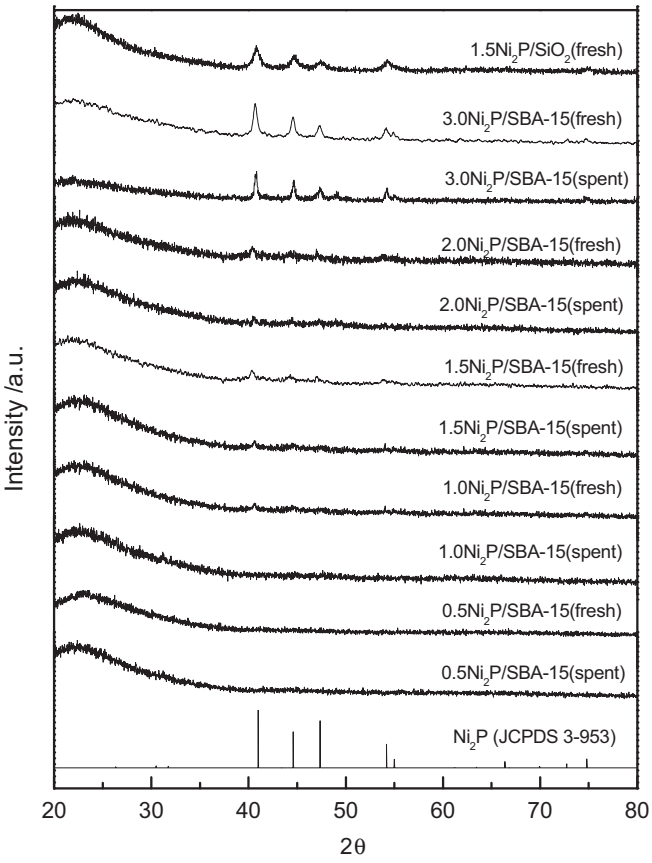

Fig. 2. XRD patterns of fresh and spent Ni_2P catalyst samples.

Ni_2P/SBA-15 and 1.5 Ni_2P/SiO_2, the peaks for a Ni_2P phase for 1.5 Ni_2P/SiO_2 was stronger than those for 1.5 Ni_2P/SBA-15, demonstrating that SBA-15 provides better dispersion for Ni_2P than low surface area SiO_2.

The physical properties of the Ni_2P catalyst samples are given in Table 2. The BET surface area of catalyst samples decreased due to a reduction in the pore volume with increasing loading levels of Ni_2P. The spent samples exhibited a partial reduction in the surface area compared with the fresh samples, which is due to the retention of reaction products on the catalysts. The TGA analysis for fresh and spent catalysts confirmed that a weight loss of ca. 20% for the spent sample was observed due to the vaporization of LCO, as presented in Fig. S1 (supplementary material). Table 2 also summarizes the elemental analysis results of the molar ratios of P/Ni and S/Ni in the fresh and spent Ni_2P samples, as determined by ICP–AES. Although the samples were prepared with an initial P/Ni ratio of 2/1, the freshly prepared samples were found to contain lower phosphorus amounts than the initial value, with the lower Ni_2P loadings retaining more P in the fresh samples of P/Ni ratios ranging from 1.32 to 0.86. In particular, it was observed that more P remained on the SBA-15 supported samples than SiO_2 supported Ni_2P catalyst. A previous work has shown that phosphorus is removed as PH_3 during the reduction procedure [21]. Similar results were also observed in a previous study on KUSY supported Ni_2P catalysts for HDS of refractory sulfur compounds [24], in which XAFS studies on the fresh and spent samples demonstrated that there are stronger interactions between Ni and P in the smaller particles, resulting in more P remaining on the catalyst after reaction. It was found that after reaction, the samples underwent further loss in P to give reduced P/Ni ratios, ranging from 0.42 to 0.84 closed to the stoichiometric value of 0.5 for Ni_2P. The catalysts also retained some sulfur after reaction (Table 2). The sulfur content was highest for the

Table 2
Physical properties of the supported Ni_2P samples.

Sample	Condition	BET surface area ($m^2\ g^{-1}$)	Pore volume ($cm^3\ g^{-1}$)		Molar ratio[c]	
			V_{micro}[a]	V_{meso}[b]	P/Ni	S/Ni
SBA-15 SiO_2	As prepared	687.3	0.045	0.705	–	–
	As received	200.0	0.010	0.380	–	–
0.5 Ni_2P/SBA15	Fresh	509.6	0.040	0.585	1.27	–
	Spent	473.4	0.025	0.558	0.75	0.20
1.0 Ni_2P/SBA15	Fresh	369.6	0.025	0.472	1.32	–
	Spent	274.5	0.020	0.369	0.56	0.06
1.5 Ni_2P/SBA15	Fresh	339.7	0.028	0.430	1.12	–
	Spent	248.2	0.003	0.362	0.84	0.06
2.0 Ni_2P/SBA15	Fresh	306.5	0.010	0.425	0.89	–
	Spent	278.8	0.002	0.367	0.84	0.01
3.0 Ni_2P/SBA15	Fresh	222.7	0.013	0.337	0.86	–
	Spent	203.3	0.001	0.180	0.71	0.03
1.5 Ni_2P/SiO_2	Fresh	123.8	0.009	0.277	1.06	–
	Spent	74.5	0.006	0.216	0.42	0.08

[a] Calculated by *t*-plot method.
[b] $V_{total}-V_{micro}$.
[c] Measured by ICP elemental analysis.

more dispersed catalysts as expected for the formation of a surface phosphosulfide on the Ni_2P.

Ni_2P particle sizes, experimental CO uptakes, and dispersions were obtained for the supported Ni_2P samples as summarized in Table 3. For the fresh samples the amount of CO uptake followed the order, 2.0 Ni_2P/SBA-15 > 1.5 Ni_2P/SBA-15 > 1.0 Ni_2P/SBA-15 > 0.5 Ni_2P/SBA-15, consistently proportional to the loading level on SBA-15 support except the case of 3.0 Ni_2P/SBA-15, indicating a poor dispersion of high loading sample. The Ni_2P/SBA-15 has a greater amount of CO uptake than Ni_2P/SiO_2 at the same loading levels of Ni_2P, indicating that the particles of Ni_2P are well dispersed on the SBA-15 support, as also will be confirmed by the TEM image results below. For the spent samples the amount of CO uptake was reduced compared to the fresh samples, especially the greatest decrease being observed for the samples with 0.5 and 3.0 loading levels, indicating the loss of active sites of the catalysts during the reaction. The Ni_2P particle sizes (D_p) were estimated from average particles sizes obtained in TEM images. Table 3 also reports the theoretical number of surface metal sites ($\mu mol\ g^{-1}$), assuming that the samples are composed of uniform spherical particles. It was calculated by the equation, surface metal sites = $S_g \times n \times f$, where S_g is the specific surface area ($m^2\ g^{-1}$) calculated from the particle size and density by the equation, $S_g = 6/(D_p \times \rho)$. The quantity n is the surface metal atom density, the number of metal atoms per unit surface, was taken here to be 1.01×10^{15} atoms cm^{-2} for Ni_2P [20,21], and f is the fractional weight loading (g of Ni_2P/g of catalyst) of the sample. The density, ρ, was taken to be 7.09 g cm^{-3} for Ni_2P [20,21]. The results of the metal site are listed in the fifth column of Table 3, and are seen to increase with increasing loading level upto 1.0, and then decrease with loading level exceeding 1.5. This is due to the growth of Ni_2P particle by the formation of aggregates with the increase of the loading level. Overall, the Ni_2P dispersion followed the order: 2.0 Ni_2P/SBA-15 > 1.5 Ni_2P/SBA-15 > 1.0 Ni_2P/SBA-15 > 3.0 Ni_2P/SBA-15 > 1.5 Ni_2P/SiO_2 ~ 0.5 Ni_2P/SBA-15, which is proportionally correlated with the amount of CO uptake for the catalysts.

Fig. 3 presents TEM micrographs of the fresh Ni_2P catalyst samples. It is evident that the SBA-15 is well synthesized with uniform hexagonal frame in pore diameter of c.a. 5 nm. The 0.5, 1.0, and 1.5 Ni_2P/SBA-15 samples retain very small particles of size smaller than 5 nm in the hexagonal support, whereas the 2.0 and 3.0 Ni_2P/SBA-15 samples have relatively large particles in size about 12 nm and larger than 23 nm, respectively, residing on the external surface of support. The particles of Ni_2P supported on SiO_2 were irregularly distributed on the surface of support, indicating poor dispersion relative to the Ni_2P/SBA-15 at the same loading levels, as also confirmed by the CO uptake results in Table 2.

EXAFS analysis is particularly useful for characterizing highly dispersed phases on supports with large surface area. Fig. 4 shows the Ni K-edge EXAFS spectra for fresh catalyst samples with different loading levels and those of a bulk reference Ni_2P sample. The EXAFS spectrum for Ni_2P comprises a little wider oscillation region in 30.0–80.0 nm^{-1} due to Ni–P contribution and a narrower oscillation region in 80.0–140.0 nm^{-1} due to Ni–Ni contribution, which gives rise to two main peaks in the Fourier transforms, centered at 0.175 nm and 0.240 nm, corresponding to Ni–P and Ni–Ni, respectively [32]. For the fresh Ni_2P/SBA-15 catalyst samples with higher loading levels of 1.5–3.0 there were also two main peaks located at almost the same positions as those of the bulk Ni_2P reference, demonstrating the presence of Ni_2P phase on the SBA-15 support, but the lower loading samples such as 0.5 Ni_2P/SBA-15 and 1.0 Ni_2P/SBA-15 presented weak Ni–Ni peak intensity, indicating that the Ni_2P phase is not well developed. These results are in well accordance with the XRD patterns shown in Fig. 2.

Fig. 5 shows the Ni K-edge EXAFS spectra for spent catalyst samples with different loading levels and those of a bulk reference Ni_2P sample. For the spent samples with higher loading levels of 1.5–3.0, two distinct peaks at 0.175 and 0.240 nm, corresponding to Ni–P and Ni–Ni, were located at almost the same position as the fresh samples, demonstrating the maintenance of Ni_2P phase during the reaction. The oscillation at 0.4–0.45 nm^{-1} became a little wider than the case of the fresh sample which implied that the spent samples were slightly bound by sulfur species to form a surface phosphosulfide during the course of LCO hydrotreating, as also observed in previous study for Ni_2P catalysts in deep hydrodesulfurization [33]. A previous study of in situ EXAFS measurements also elucidated that a Ni–S distance appears in the difference EXAFS spectra in the course of HDS, direct evidence of the formation of a surface phosphosulfide phase [34].

3.2. *Effect of Ni_2P loading on catalytic activity in LCO hydrotreating*

Light cycle oil is known to have a low cetane index (typically 15–20), and 50–80 wt.% aromatics and contain high amount of refractory sulfur compounds, i.e., alkyl DBT molecules, which makes the HDS of LCO further complicated [2,3]. The use of LCO in the diesel pool, therefore, requires deep hydrotreating to meet existing diesel fuel specifications.

Table 3
Ni_2P dispersion of the supported Ni_2P catalysts.

Sample	Condition	CO uptake (μmol g^{-1})	Particle size[a] (D_p, nm)	Surface metal site[b] (μmol g^{-1})	Dispersion[c] (%)
0.5 Ni_2P/SBA15	Fresh	26.8	3	222.4	12.0
	Spent	12.4			5.6
1.0 Ni_2P/SBA15	Fresh	63.1	5	266.9	23.6
	Spent	42.3			15.8
1.5 Ni_2P/SBA15	Fresh	73.5	8	250.2	29.4
	Spent	61.2			24.5
2.0 Ni_2P/SBA15	Fresh	89.3	12	222.4	40.1
	Spent	67.2			30.2
3.0 Ni_2P/SBA15	Fresh	58.4	23	174.1	29.2
	Spent	31.2			15.6
1.5 Ni_2P/SiO_2	Fresh	21.2	12	166.8	12.7
	Spent	10.7			6.4

[a] Calculated by TEM images.
[b] Surface metal site concentration, $S = 6/(D_p \times \rho)$.
[c] Dispersion(%) = CO uptake/mol of metal.

Fig. 6 shows the HDS conversion of LCO as a function of time on stream for the Ni_2P catalysts of different loading levels. The high loading samples of 2.0 and 3.0 Ni_2P/SBA-15 catalysts exhibited a high activity of around 98% HDS conversion at a LHSV of 0.5 h^{-1}, and maintained the activity even at higher LHSV of 1.0 h^{-1}. The 0.5, 1.0, and 1.5 Ni_2P/SBA-15 catalysts also exhibited very high and stable HDS conversion of around 88–96%, while the 1.5 Ni_2P/SiO_2 catalyst gave relatively low conversion of 84% due to a low dispersion as also confirmed by the CO uptake and dispersion results in Table 3. For the sulfide catalysts the Ni–Mo–S gave higher HDS conversion of 91% than Co–Mo–S catalyst of 78%. It is well established that the HDS of alkyl DBT molecules proceeds mainly via two parallel routes. The first route involves direct desulfurization (DDS) while the second route involves two steps; hydrogenation (HYD) of one of the aromatic rings in the first step, followed by sulfur removal as H_2S in the second step [35]. The HYD pathway is less affected by the presence of alkyl groups in the 4- and 6-positions of DBT than the DDS pathway [36]. The low activity of Co–Mo–S catalyst is due to its catalytic nature of DDS pathway being preferred rather than the HYD pathway [37]. Comparing the catalytic activity between moderate loading levels of 1.0–2.0 Ni_2P/SBA-15 and Ni–Mo–S, the Ni_2P/SBA-15 catalysts represented better HDS activity base on the same reaction conditions.

Fig. 7 compares the HDS and HDN conversion for LCO as a function of different LHSV's. The HDS activity followed the order 2.0∼1.5∼3.0»1.0 Ni_2P/SBA-15 > Ni–Mo–S/Al_2O_3 > 0.5 Ni_2P/SBA-15 > 1.5 Ni_2P/SiO_2∼Co–Mo–S/Al_2O_3 with the Ni_2P catalysts with loading levels of 2.0, and 1.5 Ni_2P having high and stable HDS conversion at around 99% even upon the increase of LHSV from 0.5 to 1.0 h^{-1}. In contrast, the HDN activity appeared slightly lower than the HDS, exhibiting the HDN conversion order 2.0 Ni_2P/SBA-15 > 1.5 Ni_2P/SBA-15 > 1.0∼3.0 Ni_2P/SBA-15 > Ni–Mo–S/Al_2O_3 > 0.5 Ni_2P/SBA-15 » Co–Mo–S/Al_2O_3 at a LHSV of 0.5 h^{-1}. Upon the increase of LHSV to 1.0 h^{-1} the HDN activity further decreased

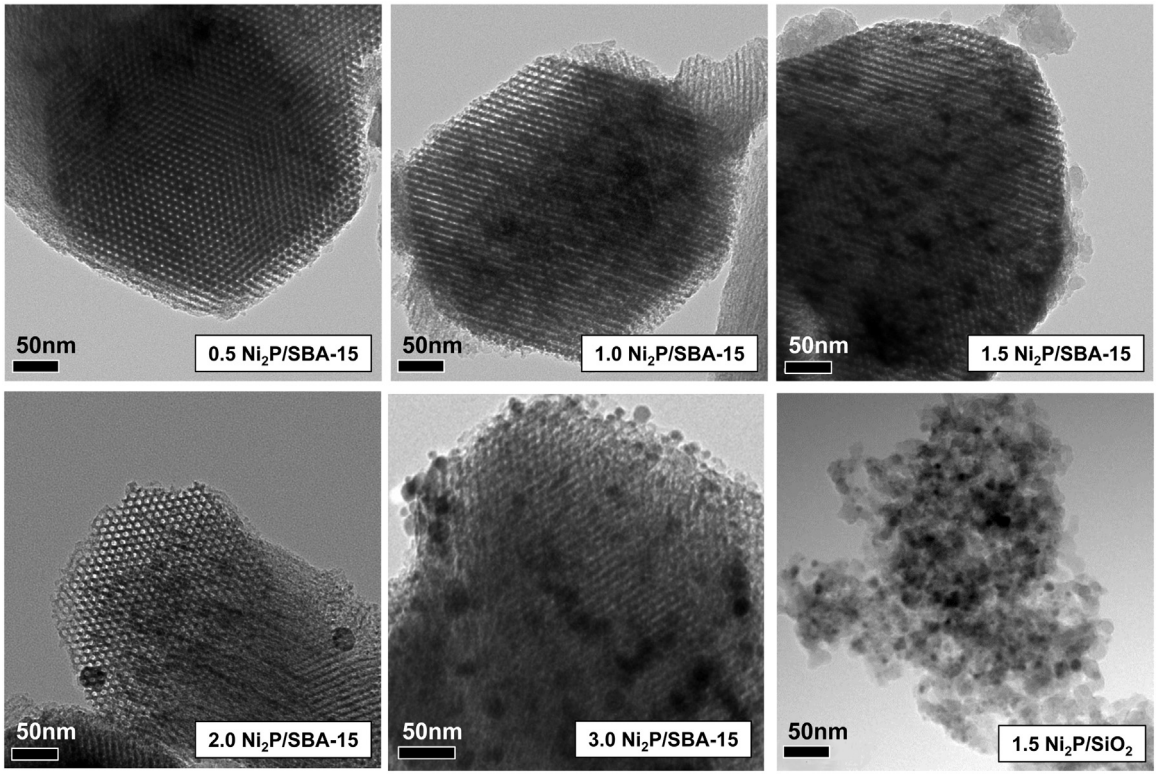

Fig. 3. TEM images of fresh catalyst samples.

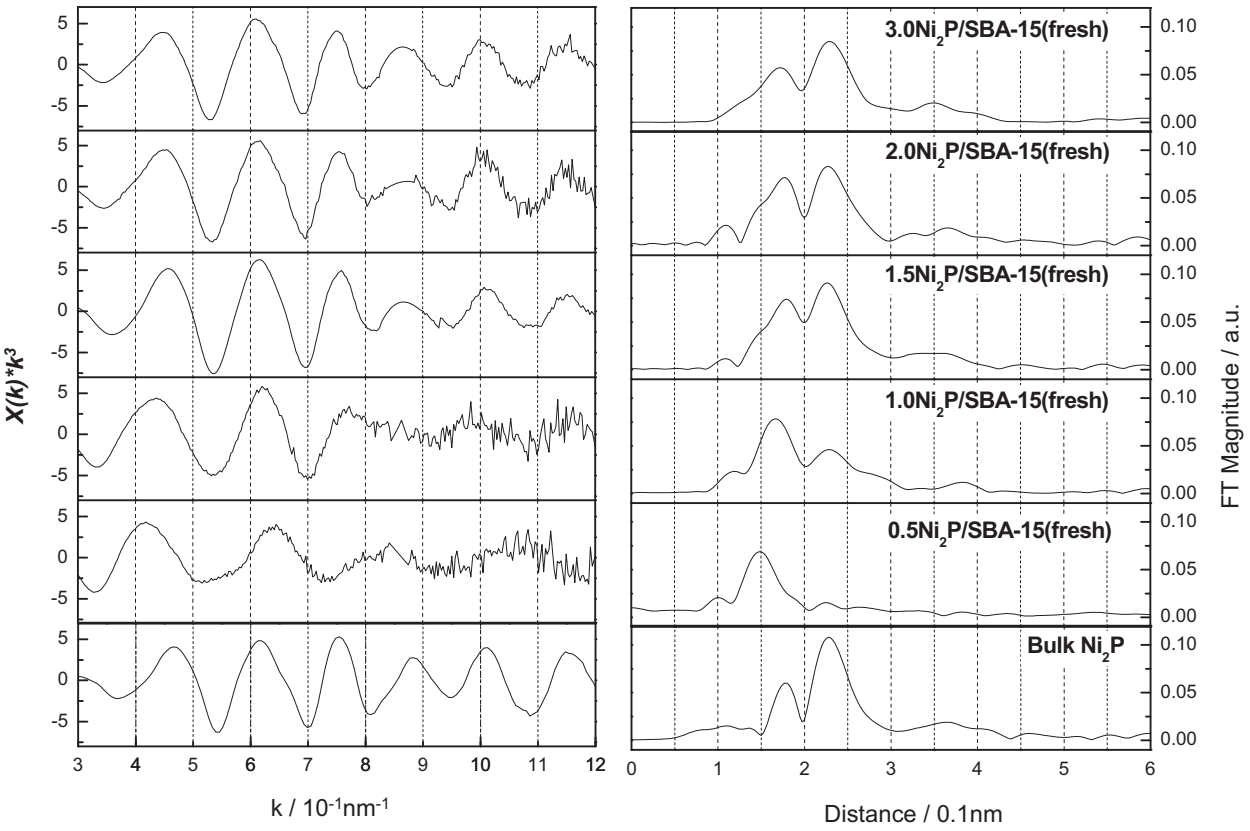

Fig. 4. Ni K-edge EXAFS spectra (left) and Fourier transform graphs (right) of fresh catalyst samples.

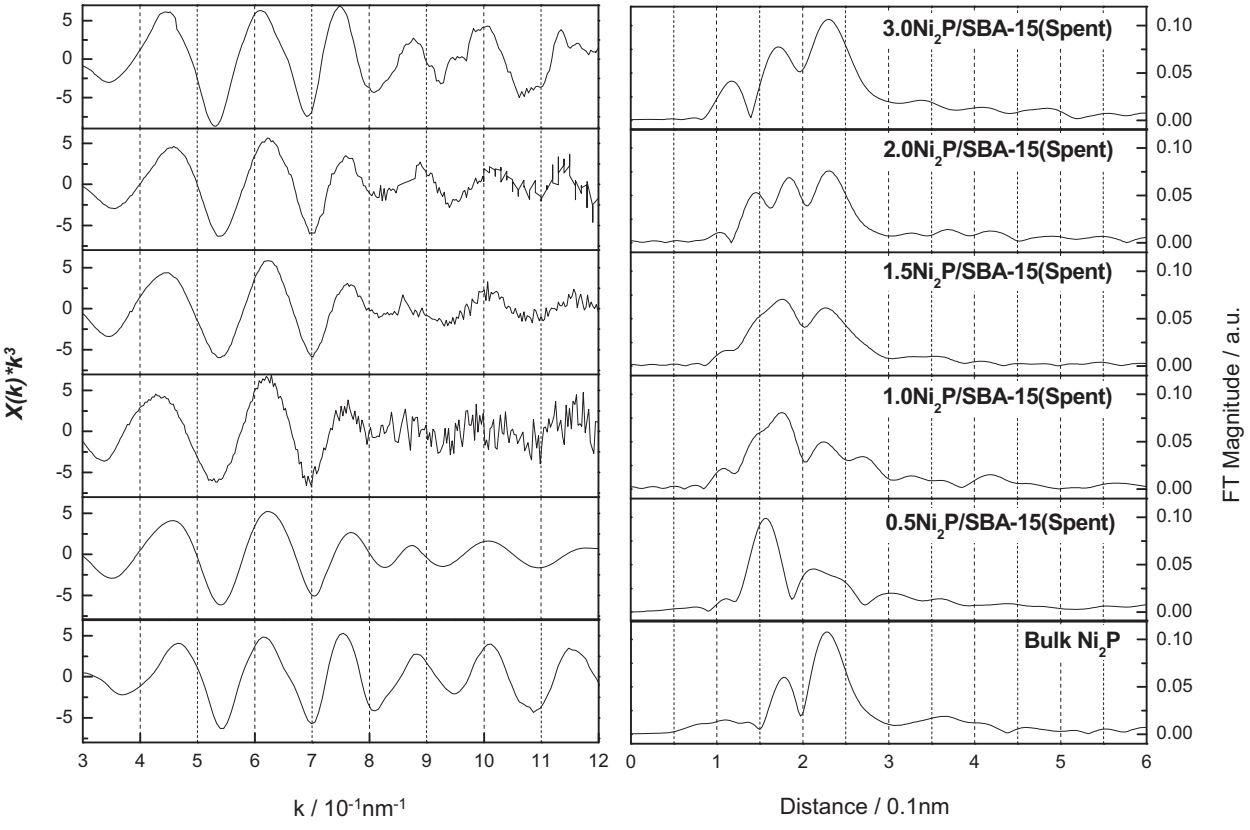

Fig. 5. Ni K-edge EXAFS spectra (left) and Fourier transform graphs (right) of spent catalyst samples.

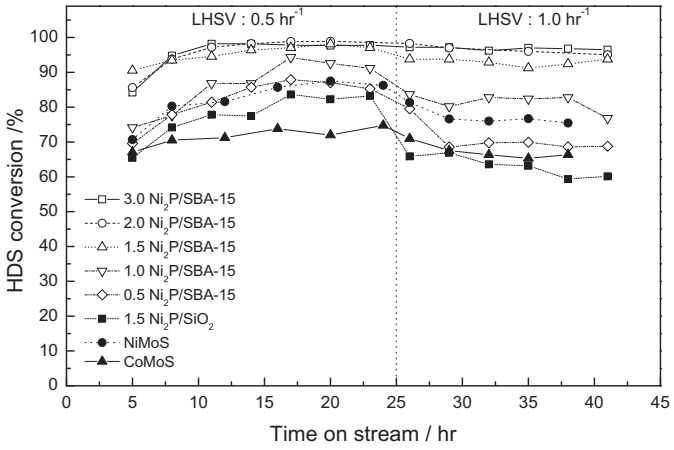

Fig. 6. HDS conversion of LCO as a function of time on stream at different LHSV's at 3.0 MPa and 623 K.

even for the highly dispersed Ni_2P samples. These results can be explained by the nature of HDN. The HDN of nitrogen compounds in oil fractions is more difficult than the HDS, requiring more severe conditions and greater hydrogen consumption due to C═N system in heterocyclic molecules. Thus, in most cases the preferred pathway for the HDN of heterocyclic molecules involves pre-hydrogenation of aromatic rings prior to a C—N bond cleavage. The different catalytic activity in HDS and HDN between sulfide and phosphide catalysts is due to the nature of the catalysts. Previous studies on deep HDS with sulfide catalysts have shown that the HDS is significantly inhibited by organic nitrogen compounds due to the competitive adsorption between nitrogen-containing compounds and sulfur-containing compounds on the catalyst active sites [38–40]. The nitrogen compounds tend to inhibit the HDS because of their strong adsorptive strength [38–40]. In contrast, Ni_2P catalysts have exhibited much better activity for HDS and HDN than a commercial Ni–Mo–S/Al_2O_3 catalyst, due to the unique nature of Ni_2P catalyst. It has been suggested that Ni_2P catalyst has a high electron density in the nickel atoms and has moderate acidity in the form of PO—H sites that are able to protonate N compounds, such as pyridine and piperidine [32,33]. These results thus suggest that the bifunctional properties of the supported Ni_2P catalyst probably contributed to the higher activity in hydrogenation and to high activity in the reaction of N and S compounds. Moreover, the 2.0 Ni_2P/SBA-15 catalyst exhibited the best activity in HDS and HDN, indicating the structure-sensitive feature of the Ni_2P catalyst for LCO hydrotreating. Similar results were reported for MCM-41-supported Ni_2P catalysts applied for deep HDS, where

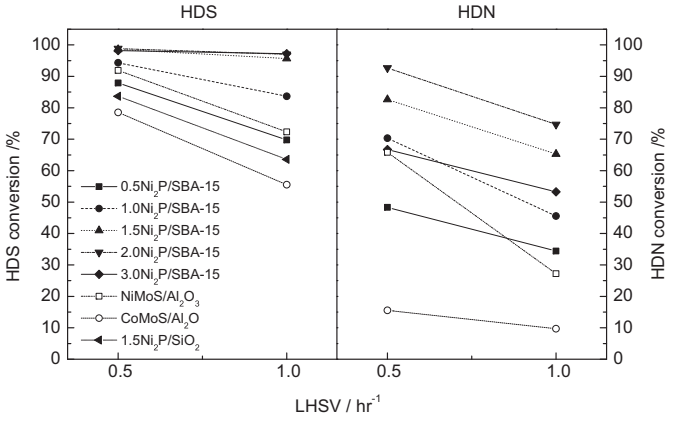

Fig. 7. HDS and HDN activity at 3.0 MPa, 623 K and different LHSV's.

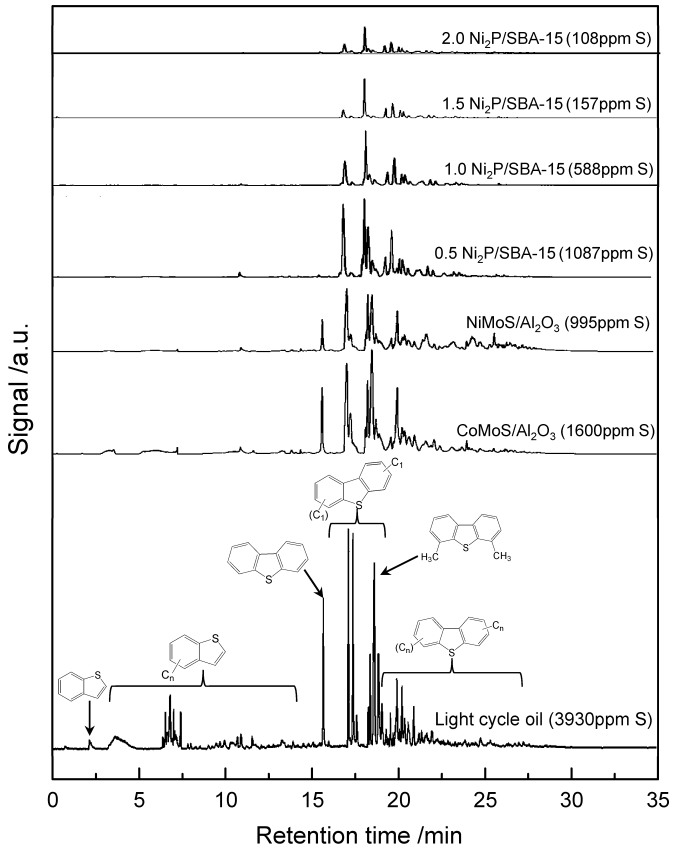

Fig. 8. GC–PFPD chromatographs of LCO feed and HDT products at 3.0 MPa, 623 K and LHSV of 1.0 h^{-1}.

the HDS conversion was strongly affected by the Ni_2P particle size. The smaller Ni_2P particles gave the better HDS activity with the HYD pathway being enhanced [23]. The higher activity of the more dispersed samples is likely due to the greater accessibility of the surface nickel atoms in the smaller particles.

Fig. 8 shows the sulfur selective GC–PFPD chromatographs of LCO feed and HDS products at 623 K, 3.0 MPa, and LHSV's of 1.0 h^{-1}. From the chromatogram of LCO it can be observed that a high percentage of sulfur are present in the alkyl derivatives of dibenzothiophene, especially dimethyldibenzothiophene (C2-DBT) which is known to react more difficultly than the derivatives of benzothiophene. The HDS activity followed the order 2.0 Ni_2P/SBA-15 > 1.5 Ni_2P/SBA-15 > 1.0 Ni_2P/SBA-15 > 0.5 Ni_2P/SBA-15, corresponding to the order of Ni_2P dispersion. Both BT's and DBT's were mostly removed over the 1.5 and 2.0 Ni_2P/SBA-15 catalysts but with a part of the DMDBT's being unconverted. These results demonstrate that the alkyl substituents sterically hinder the access of the C—S—C bond to the catalyst surface or the access of hydrogen to the C—S—C bond on the catalyst surface [37,41].

Fig. 9 shows the product distribution of the aromatic hydrocarbons for LCO hydrotreating. The LCO used in the activity test contains 74 wt.% total aromatics, among them the mono-, di-, and tri$^+$-aromatics account for ca. 15, 40, and 20 wt.%, respectively. It was noteworthy that the hydrotreating led to a substantial change in the aromatic composition, particularly over the Ni_2P catalysts. The composition of mono-aromatic hydrocarbon was gradually increased from 27 wt.% to 45 wt.% upon the consumption of di- and tri$^+$-aromatic hydrocarbons for the loading level from 0.5 to 2.0 Ni_2P. The qualitative analysis of the reaction product using GC–MS also confirmed that the hydrotreating of LCO led to the partial hydrogenation of poly-aromatic hydrocarbons to form mono- or di-aromatic hydrocarbons rather than fully hydrogenated

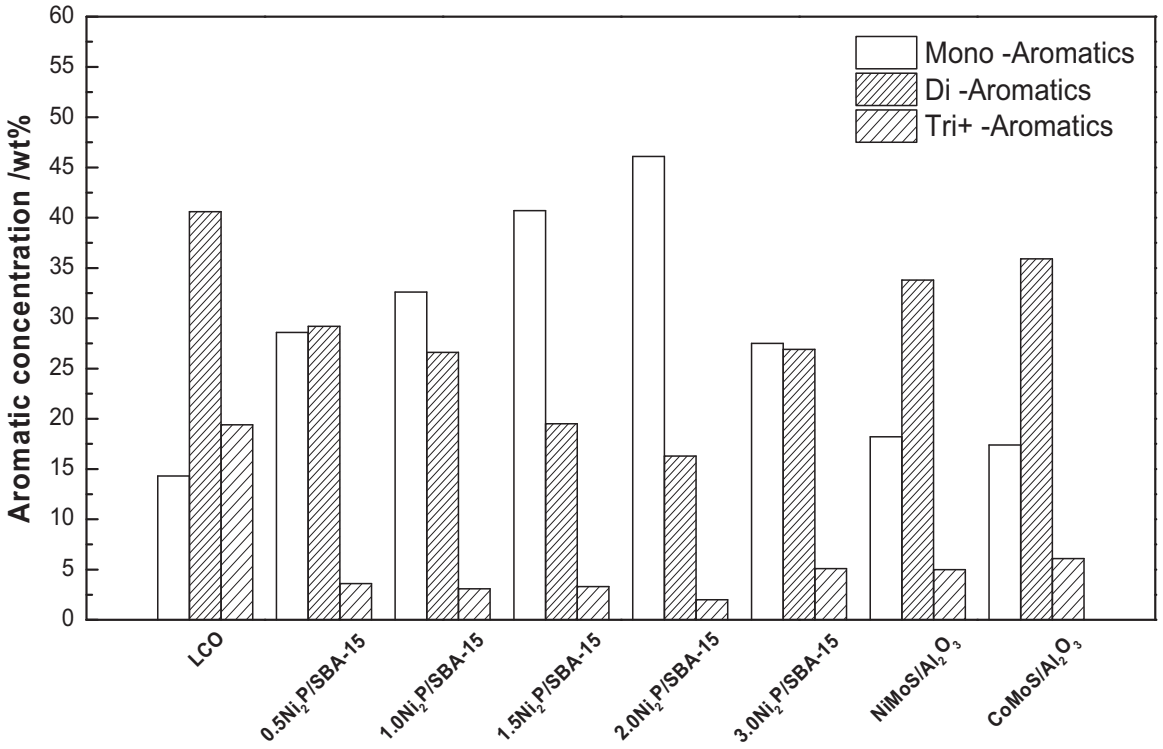

Fig. 9. Product distribution of aromatic hydrocarbons tested at 3.0 MPa, 623 K, and LHSV of 1.0 h^{-1}.

compounds like cycloalkane-derivatives at the given reaction condition (Fig. S2, supplementary material). Overall, it is obvious that the Ni_2P catalysts exhibit better hydrogenation activity to convert the poly-aromatics into mono-aromatics than that of sulfide catalysts. These results are related to the unique nature of well-dispersed Ni_2P catalysts having enhanced hydrogenation activity with a resistance toward nitrogen-compounds.

4. Conclusions

Nickel phosphide catalysts supported on SBA-15 were shown to be well suited to accomplish the desired product in the LCO hydrotreating better than conventional Ni–Mo–S/Al_2O_3 or Co–Mo–S/Al_2O_3 catalysts at 623 K and 3.0 MPa based on the equal LHSV. Among the differently loaded Ni_2P catalysts supported on SBA-15, a loading level of 2.0 mmol Ni_2P/g was found to have the best Ni_2P dispersion and exhibit the highest HDS activity at the LHSV of 0.5–1.0 h^{-1}, indicative of structure-sensitive feature of the Ni_2P catalyst for LCO hydrotreating. The HDN results also proved that 2.0 Ni_2P/SBA-15 is more active and resistant to nitrogen compounds than conventional Ni–Mo–S/Al_2O_3 and Co–Mo–S/Al_2O_3 catalysts. In particular, it was noted that the 2.0 Ni_2P/SBA-15 catalysts exhibited better hydrogenation activity for polyaromatic compounds than the sulfide catalysts with better resistance to N compounds of LCO, which contributed to the enhanced HDS and HDN activity for the refractory S and N compounds.

Appendix A. Supplementary data

Supplementary data associated with this article can be found, in the online version, at http://dx.doi.org/10.1016/j.apcatb.2014.01.010.

References

[1] V. P. Thakkar, S. F. Abdo, V. A. Gembicki, J. F. Mc Gehee, UOP Report AM-05-53 (2005).
[2] C. Song, Catal. Today 86 (2003) 211–263.
[3] P. Greening, Top. Catal. 16–17 (2001) 5–13.
[4] Y. Yoshimura, M. Toba, H. Farag, K. Sakanishi, Catal. Surv. Asia 8 (2004) 47–60.
[5] T. Fujikawa, H. Kimura, K. Kiriyama, K. Hagiwara, Catal. Today 111 (2006) 188–193.
[6] A. Stanislaus, A. Marafi, M.S. Rana, Catal. Today 153 (2010) 1–68.
[7] L. Ding, Y. Zheng, Z. Zhang, Z. Ring, J. Cheng, Appl. Catal. A 319 (2007) 25–37.
[8] H. Yang, J. Chen, C. Fairbridge, Y. Briker, Y.J. Zhu, Z. Ring, Fuel Process. Technol. 85 (2004) 1415–1429.
[9] H. Yang, J. Chen, Y. Briker, R. Szynkarczuk, Z. Ring, Catal. Today 109 (2005) 16–23.
[10] T. Song, Z.S. Zhang, J.W. Chen, Z. Ring, H. Yang, Y. Zheng, Energy Fuel 20 (2006) 2344–2349.
[11] H. Topsøe, B.S. Clausen, F.E. Massoth, in: J.R. Anderson, M. Boudart (Eds.), Hydrotreating Catalysis Science and Technology, Springer, Berlin, 1996.
[12] K.G. Knudsen, B.H. Cooper, H. Topsoe, Appl. Catal. A 189 (1999) 205–215.
[13] G. Perot, Catal. Today 86 (2003) 111–128.
[14] Z. Vít, H. Kmentová, L. Kaluža, D. Gulková, M. Boaro, Appl. Catal. 108–109 (2011) 152–160.
[15] K. Segawa, K. Takahashi, S. Satoh, Catal. Today 63 (2000) 123–131.
[16] S.T. Oyama, J. Catal. 216 (2003) 343–352.
[17] S.T. Oyama, T. Gott, H. Zhao, Y.-K. Lee, Catal. Today 143 (2009) 94–107.
[18] T.I. Korányi, Appl. Catal. A 239 (2003) 253–267.
[19] P.A. Clark, S.T. Oyama, J. Catal. 218 (2003) 78–87.
[20] P. Clark, X. Wang, S.T. Oyama, J. Catal. 207 (2002) 256–265.
[21] S.T. Oyama, X. Wang, Y.-K. Lee, K. Bando, F.G. Requejo, J. Catal. 210 (2002) 207–217.
[22] F. Sun, W. Wu, Z. Wu, J. Guo, Z. Wei, Y. Yang, Z. Jiang, F. Tian, C. Li, J. Catal. 228 (2004) 298–310.
[23] S.T. Oyama, Y.-K. Lee, J. Catal. 258 (2008) 393–400.
[24] Y.-K. Lee, Y. Shu, S.T. Oyama, Appl. Catal. A 322 (2007) 191–204.
[25] Y. Kanda, C. Temma, K. Nakata, T. Kobayashi, M. Sugioka, Y. Uemichi, Appl. Catal. A 386 (2010) 171–178.
[26] I.I. Abu, K.J. Smith, Appl. Catal. A 328 (2007) 58–67.
[27] A.W. Burns, A.F. Gaudette, M.E. Bussell, J. Catal. 260 (2008) 262–269.
[28] T.I. Korányi, Z. Vít, D.G. Poduval, R. Ryoo, H.S. Kim, E.J.M. Hensen, J. Catal. 253 (2008) 119–122.
[29] K.-S. Cho, H.-R. Seo, Y.-K. Lee, Catal. Commun. 12 (2011) 470–474.
[30] D. Zhao, Q. Huo, J. Feng, B.F. Chmelka, G.D. Stucky, J. Am. Chem. Soc. 120 (1998) 6024–6036.
[31] F. Berube, S. Kaliaguine, Micoporous Mesoporous Mater. 115 (2008) 469–479.
[32] Y.-K. Lee, S.T. Oyama, J. Catal. 239 (2006) 376–389.
[33] S.T. Oyama, X. Wang, Y.-K. Lee, W.-J Chun, J. Catal. 221 (2004) 263–273.

[34] T. Kawai, K.K. Bando, Y.-K. Lee, S.T. Oyama, W.-J. Chun, K. Asakura, J. Catal. 241 (2006) 20–24.
[35] V. Meille, E. Schulz, M. Lemaire, M. Vrinat, J. Catal. 170 (1997) 29–36.
[36] P. Steiner, E.A. Blekkan, Fuel Process. Technol. 79 (2002) 1–12.
[37] F. Bataille, J.-L. Lemberton, P. Michaud, G. Pérota, M. Vrinat, M. Lemaire, E. Schulz, M. Breysse, S. Kasztelan, J. Catal. 191 (2000) 409–422.
[38] C.N. Satterfield, M. Modell, J.A. Wilkens, Ind. Eng. Chem. Proc. Des. Dev. 19 (1980) 154–160.
[39] M. Nagai, T. Kabe, J. Catal. 81 (1983) 440–449.
[40] M.J. Girgis, B.C. Gates, Ind. Eng. Chem. Res. 30 (1991) 2021–2058.
[41] Q. Gao, T.N.K. Ofosu, S.-G. Ma, V.G. Komvokis, C.T. Williams, K. Segawa, Catal Today 164 (2011) 538–543.